

## 5. PARTICIPATION IN THE TJ-II PROGRAMME

C.A.F. Varandas and M.E. Manso (Heads), P. Coelho, L. Cupido, B. Gonçalves, A. Malaquias, L.A. Pereira,  
A. Silva, P. Varela

### 5.1. INTRODUCTION

The Portuguese participation in the TJ-II programme has been mainly focussed on the following research areas:

- Microwave reflectometry;
- Heavy ion beam diagnostic;
- Laser induced fluorescence diagnostic;
- Edge plasma physics.

An one-day meeting was held in Madrid, on October 10<sup>th</sup>, for evaluation of the results obtained in this collaboration and for discussion of the 2002 work programme.

### 5.2. MICROWAVE REFLECTOMETRY

#### 5.2.1. Main activities

The following main activities were performed:

- Development and installation of switches enabling consecutive fast broadband sweeping of the two microwave bands (Ka and Q, covering the frequency range 26-50 GHz);
- Operation of the AM section allowing the first density profile measurements to be performed;
- Tests without plasma of the FM section, which have shown an anomalous low signal to noise ratio after the first amplifier.

#### 5.2.2. Ramp switching circuit

The ramp switching circuit allows the fast ( $< 1$  ns) switching between the two microwave channels covered by the output of the HTO. The circuit is built around a fast current feedback amplifier. A simple TTL logic is used to decode the signals from the amplifier that will follow the ramp signal to the adequate HTO driver. At the same time a microwave switch uses the same decoded signals to select the input of the right frequency multiplier. The overall bandwidth exceeds 30 MHz, with a gain of one. After

the installation it became possible to use both bands in an automatic interleaved fashion. Two modifications were made leading to a significant improvement of the signals: (i) an isolator for the Ka band was removed from the circuit because it was degrading the upper band signal; (ii) the T-magic used for combining the two bands in one waveguide was replaced for 3 dB a directional coupler.

It was not possible to test the FM configuration because the microwave circuit was modified in order to optimise the AM section. The FM section will be tested with plasma as soon as the fast acquisition system with a higher sampling rate is available. A new ramp generator (possibly an AFG) is foreseen to improve the performance of the diagnostic.

#### 5.2.3. AM section

A diagram of the reflectometer front end is displayed in Figure 5.1. The system consists of a hyper-abrupt varactor-tuned oscillator (HTO) in the 12–18 GHz range in combination with active multipliers used in alternation. A dual pin switch (SPDT in Figure 5.1) is used to select between the active doubler or tripler paths, i.e. between the two frequency band segments: 25–36 GHz and 36–50 GHz. The oscillator delivers an output power of about 15 dB m. With the multipliers, power outputs of 15–20 dBm are obtained in the complete frequency range.

Two separate drivers for the HTO are used, one for each frequency band segment, allowing for an independent adjustment of the minimum and maximum frequencies and therefore permitting some overlapping in the band segments. Both drivers are controlled by a unique tuning signal, while a second control signal is used to select between the two frequency segments. A highpass filter (FHP:  $f > 36$  GHz) is included after the tripler to reduce the second harmonic (it is about 10–20 dB weaker than the third harmonic). The rejection level of the high-pass filter is of 30 dB at  $f = 34$  GHz and it is higher at lower frequencies. Therefore the second harmonic

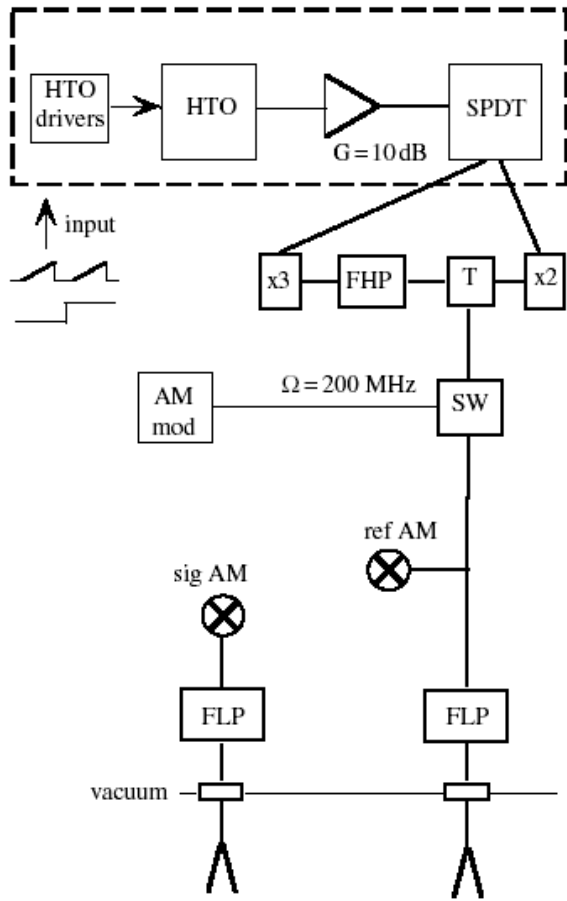


Figure 5.1 - Diagram of the AM reflectometer front end installed in TJ-II.

signal is at least 40 dB lower than the third one in the whole frequency segment.

The two paths are combined in a Tee hybrid coupler (T). Then, the signal is amplitude modulated using a single pin switch (SW) and a 200MHz modulation signal.

In the present configuration, the reference signal for the AM system can either be taken from the modulator driver or from a directional coupler installed after the modulator. This second possibility avoids the distortion introduced by the phase shift generated at the modulator that may be frequency dependent on the signal frequency. The measurements below are obtained exclusively using the signal after the modulator as the reference one. Low-pass filters (FLP:  $f_c$ : 50 GHz) have to be included to protect the system against the RF power from the ECRH system. Single-ended mixers are used to obtain the AM envelopes carrying the time delay information. Figure

5.2 shows a schematic diagram of the AM receiver. The phase demodulation of the AM signals is done at a lower intermediate frequency to achieve higher accuracy. The frequency conversion is done using a local oscillator at 189.3 MHz to obtain an intermediate frequency of 10.7 MHz. Then, band pass filters are applied to both the main and the reference signals. The present configuration has filters of 30 kHz bandwidth, though broader filters could also be used in order to increase the time resolution of the profile measurements.

The support structure of the antennas has been designed with an inclination of  $30^\circ$  from the vertical to ensure an almost pure X-mode (Figure 5.3).

The reflectometer covers almost the whole density range in all the magnetic configurations during the ECRH phase of ( $B = 1\text{T}$ ,  $f_{\text{ECRH}} = 53.2\text{ GHz}$ ,  $n_{\text{cut}} = 1.75 \times 10^{19}\text{ m}^{-3}$ ). The highest reflecting density at the magnetic axis (for the maximum incident frequency: 50 GHz) is close to  $1.4 \times 10^{19}\text{ m}^{-3}$  for most of the TJ-II magnetic configurations.

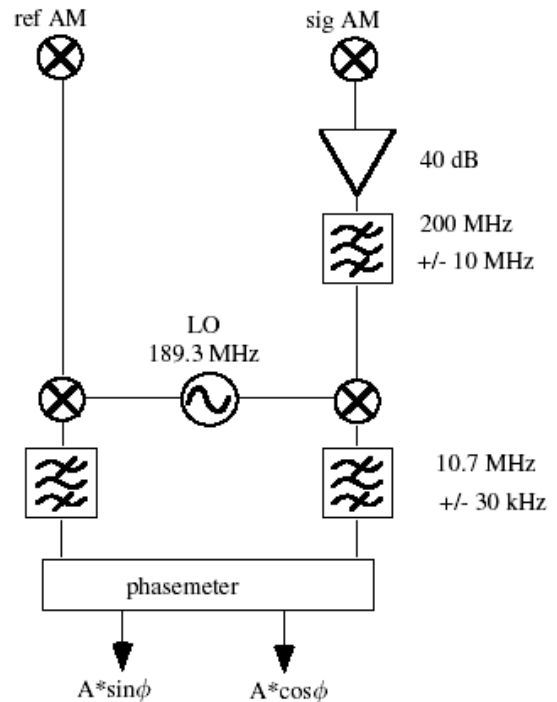


Figure 5.2 - Diagram of the AM receiver

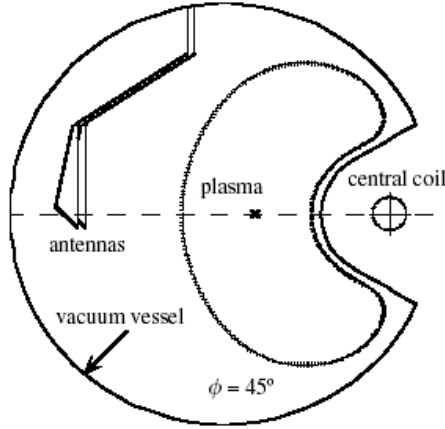


Figure 5.3 - Cross-section of the vacuum vessel and antennas and in-vessel wave-guides arrangement; the last closed magnetic surface for the standard magnetic configuration is also displayed. The broken line represents the equatorial plane of the device.

#### 5.2.4. Experimental results

The density profiles obtained by reflectometry were compared with those obtained by the high-resolution Thomson scattering system and by the lithium beam diagnostic. Taking into account that the radial range covered by the reflectometer only overlaps with that of the Thomson scattering and the lithium beam diagnostic for small sections, the agreement is in general very good (Figure 5.4).

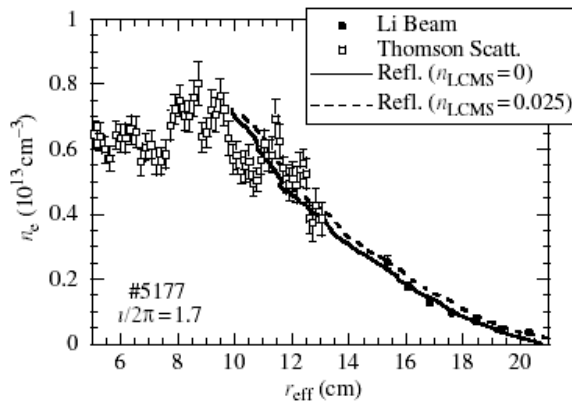


Figure 5.4 - Electron density profiles measured with three diagnostics: Thomson scattering system ( $\square$ ), lithium beam diagnostic ( $\bullet$ ) and AM reflectometer, in a plasma with low density, injected power PECH = 300kW and magnetic configuration with edge rotational transform of 1.70. The reflectometry profiles are obtained considering two different values of the density at LCMS: equal to zero (—) and equal to the density measured by the Li beam diagnostic (- - -).

In this type of discharges, the average density measured by the microwave interferometer increases continuously after the transition even when the external puffing rate decreases. Figure 5.5a) presents the average density measured by the microwave interferometer. After the transition ( $t \cdot 1150$  ms), the line average density increases continuously, reaching the ECH cut-off density at  $t \cdot 1200$  ms. Figure 5.5b) shows the evolution of the density profile measured by reflectometry. The time at which each profile is evaluated is marked by a vertical line in Figure 5.5b).

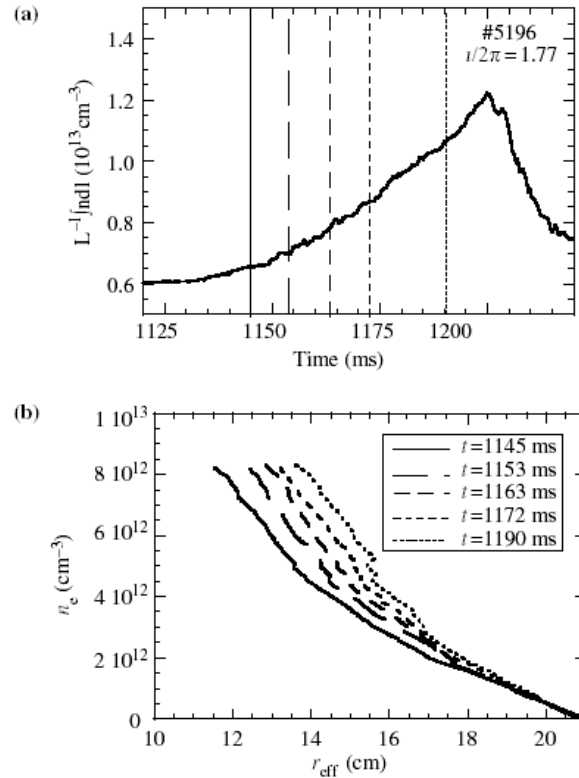


Figure 5.5 - Time evolution of the averaged electron density measured by the microwave interferometer (a) and density profiles measured by the reflectometer (b) during the transition to an enhanced confinement mode. Each vertical line in (a) represents the time at which the corresponding density profile is measured.

### 5.3. HEAVY ION BEAM DIAGNOSTIC

#### 5.3.1. Main activities

The following main tasks were made during this year:

- Improvements on the software of the dedicated control and data acquisition system;
- Design and construction in Coimbra and test at CIEMAT of a new transimpedance amplifier

aiming at matching the diagnostic operation requirements;

- Installation on the diagnostic of the first multiple cell array detector (MCAD);
- Development and installation on the diagnostic of a new MCAD based on deep Faraday cups;
- Beginning of the development of a third MCAD based on improved concept cells.

### 5.3.2. Multiple cell array detector

The first multiple cell array detector was a simple printed circuit (50x15 cm) with 120 copper cells (Figure 5.6). Experiments showed that high level of plasma loading occurs leading to a low signal to noise ratio due to the increase of photoelectrons on detector cells.

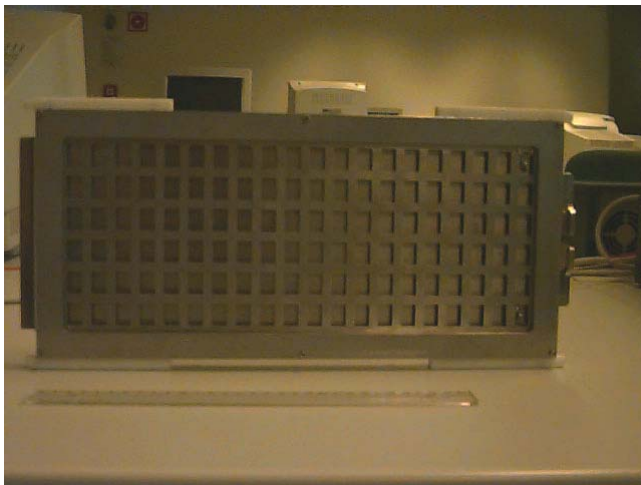


Figure 5.6 - The first Multiple Cell Array Detector (MCAD)

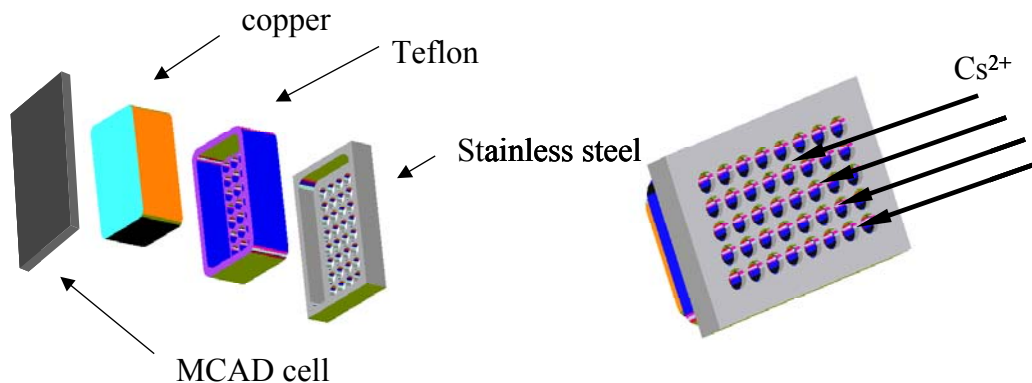


Figure 5.8 - Improved MCAD deep Faraday Cup cell

A new detector of deep Faraday cup type was developed and installed on the diagnostic. The plasma loading has decreased around 5 times when compared with that of the directed exposed cells (Figure 5.7).

Figure 5.8 shows a schematic drawing of a new MCAD, based on improved concept cells. The steel shield that is directly exposed to the plasma will be grounded to avoid space charge effects. This detector together with the increase of primary beam intensity to 100 mA will allow most probably to detect secondary ions during the 2002 campaign.

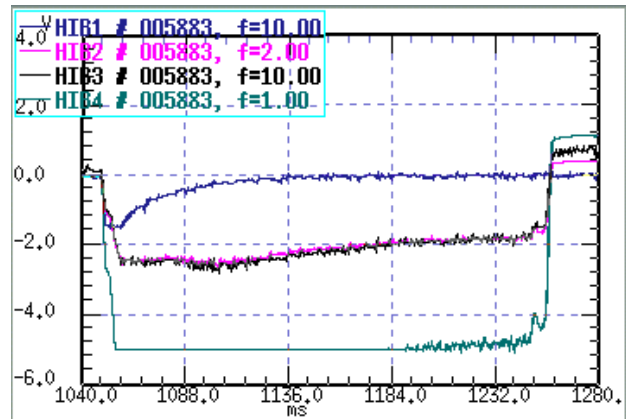


Figure 5.7 - Plasma loading signal on MCAD cells with (black) and without (pink) Deep Faraday Cup installed (signal units are arbitrary). The multiplicative factor ratio is 5. The signals look rather similar.

## 5.4. LASER INDUCED FLUORESCENCE DIAGNOSTIC

The following main activities were carried out:

- Maintenance of the dye laser and alignment of beam steering optics;
- Alignment of the detection optics and set-up of observation system;
- Analysis of a RF noise picked-up in detection electronics and attempt to achieve its suppression;
- Estimations of Rayleigh scattering for LIF diagnostic calibration in the TJ-II experiment.

## 5.5. EDGE PLASMA PHYSICS

### 5.5.1. Introduction

The activity in this research area has been focussed in 2001 on the:

- Study of the influence of the magnetic well on the plasma fluctuations and transport.

### 5.5.2. Dynamical interplay between gradients and transport in TJ-II magnetic well experiments

TJ-II was designed to have a high degree of magnetic configuration flexibility. The rotational transform can be varied between 0.9 and 2.5, allowing to perform studies on the role of magnetic topology. At the same time, the magnetic well can be changed from -1 to 6%, to study the onset of fluctuations and related phenomena close to instability thresholds. The closeness to turbulence thresholds, the type of instability driving turbulence and the presence of sheared flows are considered critical in determining the transition between different transport regimes (e.g. Bohm versus Gyro-Bohm), while self-organised critical (SOC) models predict large scale avalanches connecting remote parts of the plasma. As a consequence, the radial structure and the statistical properties of fluctuations and turbulent fluxes must be investigated. This section reports the studies on the statistical properties of plasma fluctuations and turbulent transport, varying the magnetic well in the TJ-II plasma edge region.

The absence of magnetic well (i.e. magnetic hill) gives rise in our case to instabilities at any plasma pressure. With this in mind, a sequence of configurations was selected with well depth ranging from 2.4 down to 0.2%, and having magnetic well in the bulk and magnetic hill at plasma edge, which becomes unstable. Remarkable similarity exists among those configurations according to their

rotational transform profiles as well as to their magnetic surfaces shape.

Experiments were carried out in ECRH plasmas, using one or the two gyrotrons of TJ-II heating system (PECRH = 300 – 600 kW). A fast reciprocating Langmuir probe has been used to investigate the structure of plasma profiles and their fluctuations. Fluctuations in the ion saturation current, floating potential and ExB turbulent fluxes, together with their degree of intermittence, have been observed to get higher when magnetic well is reduced. The greatest increase in the level of fluctuations occurs when reducing the well from 2.4 to 0.9% what may suggest an instability threshold somewhere in-between those levels.

The probability density distribution of density gradient is rather gaussian despite of the well (Figure 5.9). However, a broadening of the distribution appears with a decrease of the magnetic well and associated to the increase of fluctuation level. The most probable value of density gradient exhibits a minimum on turbulent flux amplitude. It is possible to see that the decrease of magnetic well allows the plasma to explore more of the expected ExB flux curve. Most of the time the plasma is in a minimum flux state.

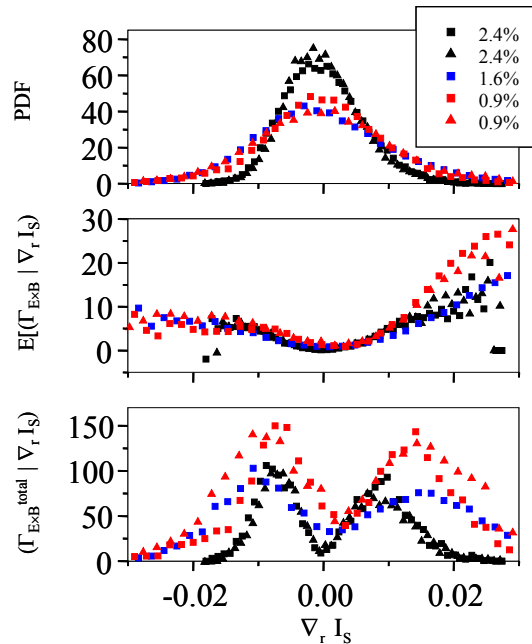


Figure 5.9 - a) The probability distribution function of gradient with different magnetic well; b) Expected turbulent flux at a given density gradient. The most probable value of density gradient minimizes flux events amplitude; c) Most of the transport occurs when the plasma leaves the most probable value.

As revealed by the bi-coherence analysis the decrease on magnetic well increases the amount of non-linear transfer on ion saturation current (Figure 5.10). Both results are consistent with the concept of

transport self-regulated through ExB flows driven by fluctuations near marginal stability.

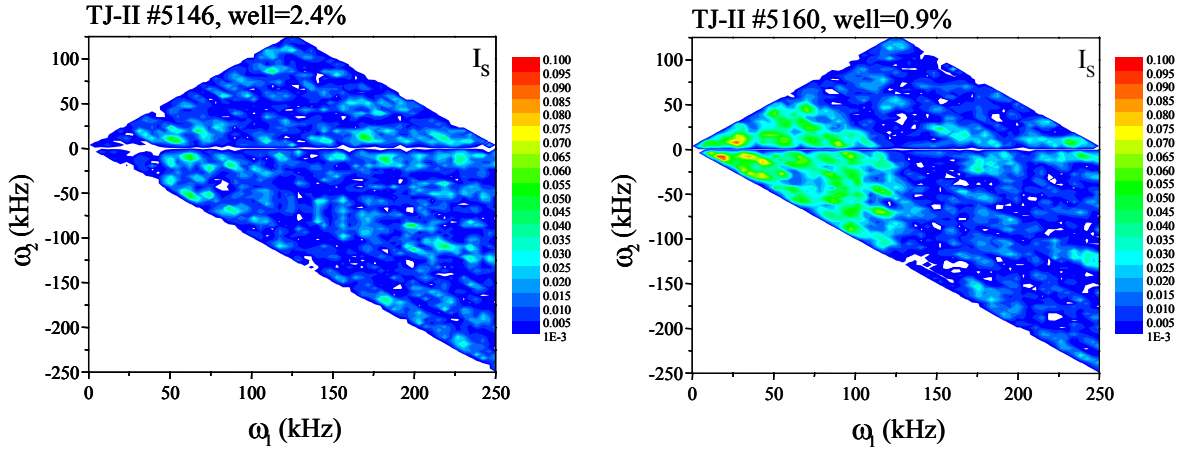


Figure 5.10 - Ion saturation current bi-coherence with different magnetic well. The decrease on the magnetic well leads to an increase on non-linear energy transfer between distinct frequencies.